Impacts of Convective Lifetime on Moist Geostrophic Adjustment

JULIANA DIAS AND OLIVIER PAULUIS

New York University, New York, New York

(Manuscript received 8 December 2009, in final form 3 May 2010)

ABSTRACT

This paper presents a theoretical study of the effects of moist convection on geostrophic adjustment in an infinite channel. The governing equations correspond to a linearized shallow water system of equations for the atmosphere first vertical baroclinic mode, which is coupled to a vertically averaged moisture equation. The coupling is through a parameterization that represents precipitation. The transient behavior and final state of the flow initially at rest with active precipitation limited to half of the channel is investigated, both numerically and analytically. It is shown that an initial imbalance resulting from precipitation induces a circulation that dries out the nonprecipitating region and further enhances precipitation. This interaction between precipitation and dynamics leads to a sharper temperature gradient and stronger jet in the final state, when compared to the dry adjustment. Unlike in the dry case, the moist geostrophic adjustment cannot be entirely determined from the initial unbalanced flow, since it depends on the time scale for convection. Analytic approximations are derived in limits of both fast and slow convective adjustment time.

1. Introduction

The geostrophic adjustment problem for rotating fluids is an initial-value problem where an unbalanced flow evolves toward a balanced state defined by the equilibrium between Coriolis and pressure gradient forces. The relationship between the initial and the final balanced states was first studied by Rossby (1938) and a review on the geostrophic adjustment problem can be found in the paper by Blumen (1972). Perhaps the simplest example of geostrophic adjustment is the one on an infinity channel, where a rotating shallow water fluid is initially at rest with a step profile in temperature. The flow evolves toward a final state where the velocity field balances the temperature gradient (Gill 1982). In this case, the final state is achieved after inertia–gravity waves propagate away from the initial disturbance, carrying energy away from the system. Therefore, the end state energy is less than the initial state by the amount of energy carried away by inertia–gravity waves. Importantly, the final state can be obtained analytically from the initial condition, and so can the energy partition between geostrophic and ageostrophic modes.

The atmosphere can be seen as a mixed fluid composed of dry air and water, in which fluctuations in velocity and temperature are associated with fluctuations in precipitation through latent heating due to water phase transitions. The atmospheric geostrophic adjustment to stationary and transient heat sources has been previously investigated (Gill 1980; Silva Dias et al. 1983) and it has been shown that the energy contribution to the transient adjustment by gravity waves depends on the spatial and temporal distribution of the forcing. Although these models provide relevant simulations, they have the limitation that they do not include the feedback between circulation and precipitation. To address this limitation, Emanuel et al. (1994), based on the quasi-equilibrium (QE) assumption (Arakawa and Schubert 1974), argue that the effect of convection on the large-scale circulation is to reduce the effective static stability of the atmosphere. Building on this approach, Frierson et al. (2004, hereafter FMP) developed an idealized framework to study the feedback between water vapor and large-scale circulation that allows for interactions between precipitating and nonprecipitating regions. The model by FMP has been previously used to study the propagation of precipitating regions (Stechmann and Majda 2006; Pauluis et al. 2008) and to investigate the propagation of convectively coupled equatorial waves (Dias and Pauluis 2009).

Corresponding author address: Juliana Dias, New York University, 251 Mercer St., New York, NY 10012.
E-mail: dias@cims.nyu.edu

DOI: 10.1175/2010JAS3405.1

In the present work, we use the model by FMP to study the impacts of convective lifetime on the geostrophic adjustment process. Observational studies such as Betts (1986) suggest a convective adjustment time between 2 and 12 h, while the Coriolis parameter varies from 0 s^{-1} at the equator to 10^{-4} s^{-1} in the midlatitudes. Thus, it is important to understand the effects of the separation between these two time scales, both for the transient and for the balanced flow. To investigate the mechanisms of the adjustment we integrate the model by FMP on an f plane and in one space dimension, analyzing the adjustment for different ratios of precipitation and rotation time scales in comparison to the dry geostrophic adjustment.

Physically, the ratio between convective and geostrophic adjustment time can be seen in two ways. On the one hand, when the convective adjustment time is fixed, the comparison between time scales can be thought as the effects of moist convection on the geostrophic adjustment closer or farther from the equator. On the other hand, when the rotation frequency is fixed, the impact on the geostrophic adjustment of a shorter or longer convective adjustment time can be compared at a fixed distance from the equator.

The effects of convective lifetime on balanced flows is presented in the context of a geostrophic adjustment process in an infinite channel that is initially precipitating on one-half of it and dry on the other half. This paper is organized as follows. Section 2 reviews the governing equations and equations for the moist and dry potential vorticity (PV) are derived. Unlike the traditional baroclinic adjustment problem, because dry PV is not conserved, the final balanced flow cannot be determined from the initial PV field. To illustrate that, the initial-value problem is presented in section 3. In particular, the transient behavior and the final state are described for different ratios of convective and geostrophic adjustment time. In section 4, the mechanisms of the adjustment are analyzed and we derive approximations for the final state in two limiting cases, fast and slow convective adjustment time compared to the earth's rotation time scale. In the last section we summarize the main results.

2. Modeling framework

The model used here is equivalent to the Quasi Equilibrium Tropical Circulation Model (QTCM) from Neelin and Zeng (2000), and it is based on a Galerkin truncation of the hydrostatic Boussinesq equations, where only the barotropic and first baroclinic modes are retained. To allow the flow to affect the precipitation distribution, the motion equations are coupled to an equation for the vertically integrated mixing ratio of water vapor in the atmosphere (moisture), utilizing a quasi-equilibrium relaxation for precipitation closure. More specifically, the zonal wind is given by $U = \overline{U}(x, y, t) + u(x, y, t)\Psi_u(z)$, the meridional wind is given by $V = \overline{V}(x, y, t) + v(x, y, t)\Psi_v(z)$, the temperature $T = \overline{T}(z) + T(x, y, t)\Psi_T(z)$, the vertical velocity $W = w(x, y, t)\Psi_w(z)$, and the moisture $q = \overline{Q}(z) + q(x, y, t)$. The quantities $\overline{T}(z)$ and $\overline{Q}(z)$ are the horizontally uniform temperature and moisture profiles, and $q(x, y, t)$ is the vertically averaged moisture. The vertical velocity is assumed to be zero at the surface and tropopause. The first baroclinic vertical structure is then given by $\Psi_u(z) = \Psi_v(z) = \cos(z)$ and $\Psi_T(z) = \Psi_w(z) = \sin(z)$, where the height of the tropopause H_T was nondimensionalized to π. The vertical structure functions were chosen so that the vertical derivative of Ψ_T and Ψ_w are equal to Ψ_u and Ψ_v. In particular, the continuity equations can be written as

$$\frac{\partial}{\partial z}[w(x, y, t)\Psi_w(z)] = -\frac{\partial}{\partial x}[u(x, y, t), \Psi_u(z)] - \frac{\partial}{\partial y}[v(x, y, t), \Psi_v(z)] \rightarrow$$

$$w = -\nabla_H \cdot \mathbf{u},$$

where the horizontal gradient is $\nabla_H = (\partial_x, \partial_y)$ and (x, y, z) represent the zonal, meridional, and upward distances.

Although keeping the barotropic wind $\overline{U}$ is important, particularly for the study of tropical–extratropical interactions, to simplify the study of the active role of moisture in the context of balanced flows we assume here that there is no barotropic wind. In the absence of barotropic wind, the model consists of a shallow water system coupled to an equation for moisture. The full derivation of this model is available in FMP, which is itself adapted from Neelin and Zeng (2000). In section 2a, the governing equations are reviewed, and a discussion of the convective parameterization is presented. The equations for the dry and moist potential vorticity are derived in section 2b and the equations for the balanced flow in section 2c.

a. Governing equations

Since the goal is to analyze the time evolution of an initially unbalanced fluid in an infinite channel, the initial state is chosen to be independent of y and the Coriolis parameter is constant. The flow remains independent of y for all times; hence, we present only the one-dimensional model. In this case, in the absence of the barotropic flow and on the f plane, the nondimensional flow equations from FMP are

$$\partial_t u - \partial_x T - fv = 0, \tag{1a}$$

$$\partial_t v + fu = 0, \tag{1b}$$

$$\partial_t T - \partial_x u = P. \tag{1c}$$

The time scale used is $\hat{t} = 1/f$ and the length scale is $\hat{L} = c_d/f$, with the characteristic speed given by $c_d^2 = \pi^{-1} H_T C_p \partial_z \overline{T} + g H_T$, where C_p is the heat capacity at constant pressure. The diabatic forcing in the temperature Eq. (1c) represents the precipitation rate P. To close the system, in the FMP formulation, an equation for the vertically integrated moisture is derived:

$$\partial_t q + \tilde{Q} \partial_x u = -P, \tag{2}$$

which is scaled by the nondimensional quantity $C_p T_0/L_v$, where T_0 is the temperature scale and L_v is the latent heat of vaporization. A key assumption in this derivation is that the gross moisture stratification $\tilde{Q}$ depends only on the reference moisture profile $\overline{Q}(z)$, which is obtained from a mean sounding. Hence, the moisture gradient depends only on the background moisture, and the term $\tilde{Q}\partial_x u = -\tilde{Q} w$ represents advection of moisture. The parameter $\tilde{Q}$ is positive since typical moisture soundings fall exponentially with height, and it is less than one for a typical mean sounding. Here, we fix $\tilde{Q} = 0.9$, corresponding to a background moisture gradient of 1.75 g kg^{-1} km^{-1}.

In comparison to the QTCM, FMP further simplifies the model by assuming that the vertical average of moisture is only advected by the barotropic flow. The main model parameters and scales are summarized on Table 1. Note that since we consider that $\overline{U} = 0$, in this case the model has no horizontal advection of moisture. This approximation can be refined; however, it adds a level of complexity since the model would have a quadratic nonlinearity. While the detailed effects of a baroclinic moisture advection merit further investigation, we do not include this term in the present work.

The precipitation parameterization used in the QTCM stands on the Betts and Miller (1986) formulation in which convection is active when moisture exceeds a reference saturation profile and it is then relaxed to the saturation value $\hat{q}$ over a given time scale. In regions where moisture is below saturation, convection is inactive and precipitation vanishes. Mathematically,

$$P = \max\left(\frac{q - \hat{q}}{\tau_c}, 0\right), \tag{3}$$

where τ_c is the convective adjustment time. For a given saturation value $\hat{q}$ a new moisture variable can be defined as $q' = q - \hat{q}$, and with this change of variables an equivalent set of equations is obtained where $\hat{q} = 0$.

TABLE 1. Model parameters and scales.

Parameter	Value	Description
H_T	16 km	Tropopause height
f	10^{-4} s	Coriolis parameter
τ_c	2–12 h	Convective adjustment time
T_0	15 K	Temperature scale
$\partial_z \overline{Q}(z)$	1.75 g kg^{-1} km^{-1}	Background moisture gradient
c_d	50 m s^{-1}	Dry gravity wave speed
c_m	15 m s^{-1}	Moist gravity wave speed
L_d	490 km	Dry Rossby radius
L_m	150 km	Moist Rossby radius
$C_p T_0/L_v$	6×10^{-3}	Scale factor for moisture

Hence, hereafter we consider only the case $\hat{q} = 0$; that is, negative values of moisture should be interpreted as the vertically integrated moisture content being below saturation, in which case precipitation is inactive. Conversely, in a region where $q > 0$, precipitation is active. The problem remains nonlinear because of the transition between precipitating $P > 0$ and the nonprecipitating regions where $P = 0$, which represents the interface between moist and dry regions. Importantly, in FMP energy equations are derived including a quantity that can be interpreted as a moist available potential energy, and it is shown that the entire system is dissipative, independent of the convective adjustment time.

b. Moist and dry potential vorticity

The relative vorticity is $\zeta = \partial_x v$ and the dry and moist potential vorticity are defined by

$$\eta_d = \zeta + fT, \tag{4a}$$

$$\eta_m = \zeta + \frac{f}{1 - \tilde{Q}}(T + q). \tag{4b}$$

Differentiating Eq. (1b) with respect to x and combining with Eqs. (1c) and (2) yields

$$\partial_t \eta_d = fP, \tag{5}$$

$$\partial_t \eta_m = 0. \tag{6}$$

Note that since $P \geq 0$, the amplitude of the dry PV increases when precipitation is active, whereas the moist PV is conserved.

c. Geostrophic balanced state

In this formulation, the geostrophically balanced flow satisfies $u_F = 0$, $v_F = -\partial_x T_F/f$, $P_F = 0$, and

$$\eta_{d,F} = -\frac{\partial_{xx} T_F}{f} + \frac{f}{c_d^2} T_F, \tag{7a}$$

$$\eta_{m,F} = -\frac{\partial_{xx} T_F}{f} + \frac{f}{c_m^2}(T_F + q_F), \tag{7b}$$

where the subscript F stands for variables at the final steady state, $c_d = 1$ is the nondimensional gravity wave speed, and $c_m = \sqrt{1 - \tilde{Q}}$ is the moist gravity wave speed as defined in FMP. Note that because at final state $P_F = 0$, the final moisture distribution q_F has to be below saturation. In addition, time integration of Eqs. (5) and (6) gives a relation between the initial and final potential vorticity

$$\eta_{d,F} = \eta_{d,I} + f\langle P\rangle, \tag{8a}$$

$$\eta_{m,F} = \eta_{m,I}, \tag{8b}$$

where the subscript I stands for variables at initial time and $\langle P\rangle = \int_{t_I}^{t_F} P\,dt$ is the total precipitation. The balanced temperature can be determined both through inversion of Eq. (8a) using (7a), or through inversion of Eq. (8b) using (7b). Using the dry potential vorticity formulation, the inversion requires knowledge of the total precipitation $\langle P\rangle$, whereas using the moist potential vorticity it requires knowledge of the final distribution of moisture q_F. In fact, the two formulations are equivalent since time integration of (1c) and (2) yields

$$\langle P\rangle = -\frac{(q_F + \tilde{Q}T_F) - (q_I + \tilde{Q}T_I)}{1 - \tilde{Q}}. \tag{9}$$

Notice that if there is no precipitation—that is, if the initial value of q is sufficiently negative—the final temperature can be determined from the initial data. Thus, in contrast to the dry geostrophic adjustment problem, Eq. (8a) suggests that we cannot determine the final state given only the initial state of the flow. To illustrate the effects of moist convection in the geostrophic adjustment process, in the next section we numerically integrate the governing Eqs. (1), given a particular choice of initial conditions, and in section 4 we discuss the physical mechanisms of the adjustment process.

3. Numerical simulations

Numerical solutions are obtained utilizing the nonoscillatory balanced scheme introduced by Khouider and Majda (2005a) and Khouider and Majda (2005b). To avoid reflection of gravity waves at the boundaries, we work on a very large domain with the adjustment region ($\sim 10L_d$) located at its center. Moreover, we stop integrations before any reflected wave could enter the region of interest. The domain corresponds to a latitude line of size $2L_c$ (i.e., $x \in [-L_c, L_c]$ where L_c is large compared to the Rossby radius $L_d = c_d/f$).

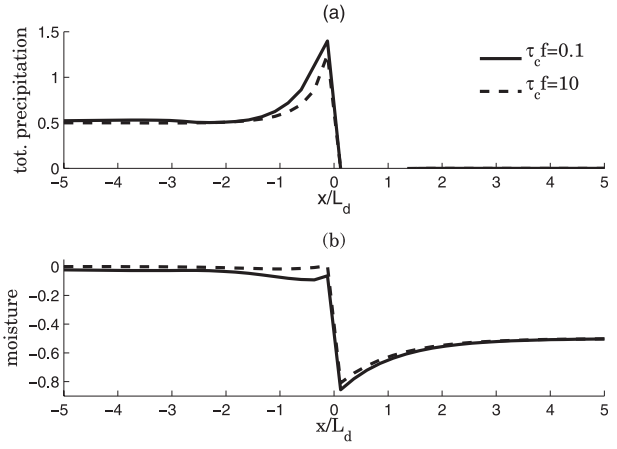

FIG. 1. (a) Time-integrated precipitation for $\tau_c f = 0.1$ (solid) and $\tau_c f = 10$ (dashed). (b) As in (a), but for the final moisture distribution.

Since the adjustment depends on both the initial state and the convective adjustment time τ_c, here we compare an initial value problem for $\tau_c = 0.1/f$, $\tau_c = 1/f$, and $\tau_c = 10/f$. In this problem we initialized the model with a motionless atmosphere, with a uniform distribution of temperature and a step profile in the initial moisture content. In particular, to the left of the origin the domain is initially supersaturated and to the right it is unsaturated. The portion of the domain that is initially unsaturated remains unsaturated throughout the adjustment process (see Fig. 1a).

The propagation of gravity waves away from the initial discontinuity is illustrated in Fig. 2. It is noticeable that the propagation speed is slower to the left than to the right of the discontinuity when $\tau_c = 0.1/f$ (left panels) than when $\tau_c = 10/f$ (right panels). The initial discontinuity in the moisture content triggers precipitation to the left of the origin and the initial precipitation is stronger when τ_c is shorter (bottom panels). The total amount of precipitation shows a similar behavior in both cases, except that when τ_c is shorter it precipitates more, as can be seen in Fig. 1a, which is associated with a final moisture distribution below saturation even in the initially moist portion of the channel, as shown in Fig. 1b.

The final balanced state is shown in Fig. 3, where it is compared to the dry geostrophic balance solution (thin dotted line). The two moist cases have in common a stronger jet due to the stronger temperature gradient and the loss of symmetry due to the asymmetric precipitation distribution illustrated in Fig. 1a. Precipitation acts as a heat source; thus, the final temperature is higher than in the dry case everywhere in the channel. However, since precipitation is never active on the right portion of the domain, temperature is smooth and

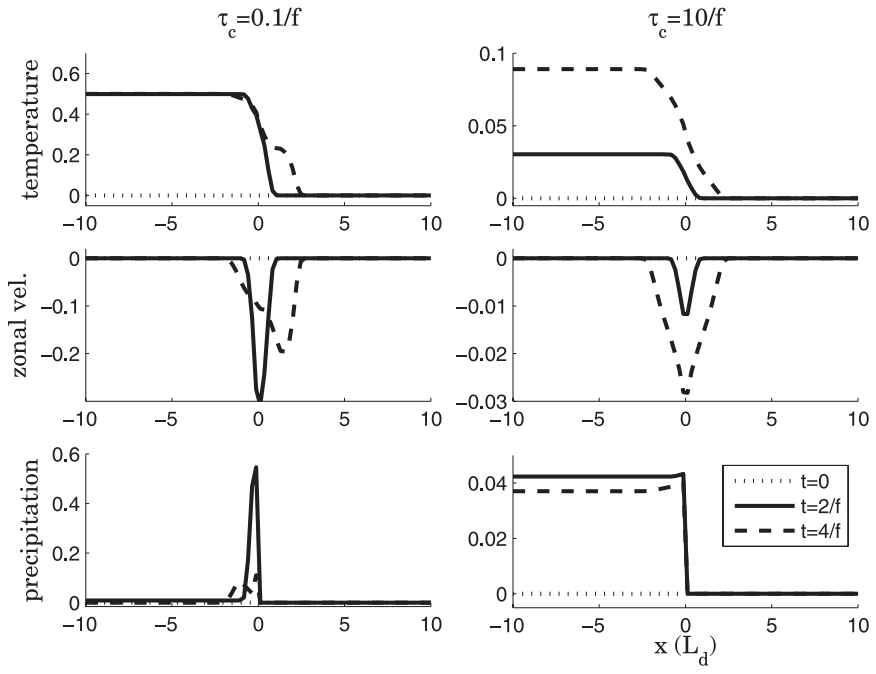

FIG. 2. Initial adjustment for $q(0, x) = -q_0 \,\mathrm{sign}(x)$ ($q_0 = 0.5$): (top) temperature, (middle) zonal velocity, and (bottom) precipitation: (left) $\tau_c = 0.1/f$, (right) $\tau_c = 10/f$. The thin dotted line corresponds to variables at $t = 0$, the thick line to $t = 2/f$, and the dashed line to $t = 4/f$.

comparable to the dry analytical solution for all values of τ_c.

Although Fig. 3 indicates that the latent heat initially released at the discontinuity sharpens the final temperature front independently of the relation between τ_c and f, the initial burst of precipitation has a distinct effect depending on the ratio between the two time scales. When τ_c is short, the final adjusted solution shows a bump in temperature near the maximum precipitation location and the amplitude of the bump increases with decreasing τ_c. When the convective adjustment is slow compared to rotation, the total precipitation and the final solution are smoother. In fact, the final temperature is similar to the dry solution for a shorter length scale to the left of the origin. In the next section we turn to the analysis of the two limiting cases: short and long τ_c.

4. Adjustment in the slow and fast convective limit

Based on observational studies that have suggested a convective adjustment time between 2 and 12 h (Betts 1986), the parameter $\tau_c f$ ranges from 0.1 near the equator to 4.0 in the midlatitudes, as can be seen in Fig. 4. Hence, in theory, the limiting behaviors $\tau_c f \gg 1$ (slow convective limit) and $\tau_c f \ll 1$ (fast convective limit) described in the previous section can be observed. In this section, we first explore the similarities between the slow and fast convective limits. Next, in sections 4b and 4c, we separately analyze the distinct characteristics of the two limiting cases. The focus of the discussion is on both the transient flow ($t \ll 1/f$) and the final balanced state. Remarkably, we find that in both limits the final state flow can be estimated from the initial flow.

a. Similarities of the moist geostrophic adjusted flow

The results from the previous section indicate that the adjustment to the unbalanced initial moisture distribution triggers precipitation to the left of the edge of the

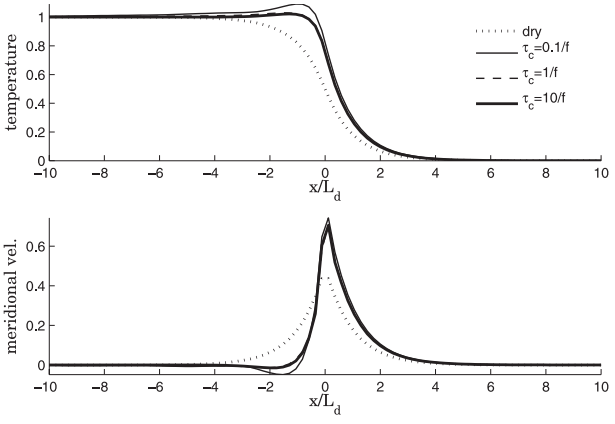

FIG. 3. Comparison between final balanced state when $q(0, x) = -q_0 \,\mathrm{sign}(x)$ for $\tau_c f = 0.1$, 1, and 10, and the dry case (thin dotted line). All variables where normalized such that $\Delta q(x, 0) = 1$.

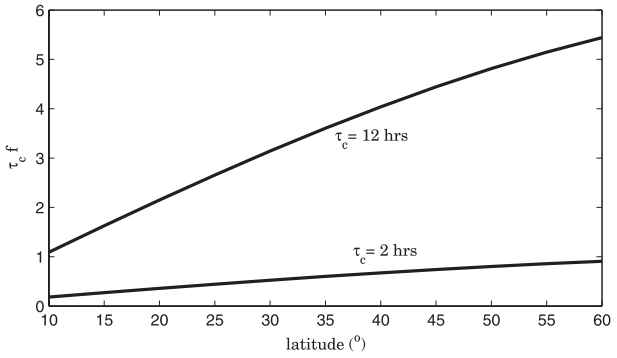

FIG. 4. Scale $\tau_c f$ as a function of latitude for two fixed values of τ_c. The top line corresponds to $\tau_c = 12$ h and the bottom line to $\tau_c = 2$ h.

initially supersaturated region. Latent heat is released in this region and temperature rises; hence, the final balanced flow exhibits a sharper temperature front, and a sharper jet, than the equivalent dry system would have. In this section, in order to clarify the physical mechanisms of the moist geostrophic adjustment process, we carry on a careful investigation of the adjustment shortly after the beginning of the integration time ($t \ll 1/f$).

Initially, the precipitation P is uniform to the left of the origin and vanishes to the right of it ($P = 0$ for $x > 0$). Using linear approximation in space and time, we obtain a scaling for the amplitude of the temperature to the left of the origin:

$$T(0^-, \Delta t) \approx q_0 \frac{\Delta t}{\tau_c}, \tag{10}$$

where the superscript "$-$" indicates the region to the left of the origin.

As the temperature rises in the moist region, it generates a gradient of temperature near the origin, which drives a direct circulation with air flowing toward the warm, moist regions near the surface and toward the dry regions in the upper levels. Linear approximation of the momentum equation yields a scaling for the amplitude of the zonal wind:

$$u(0, \Delta t) \approx -q_0 \frac{\Delta t^2}{\Delta x \tau_c}, \tag{11}$$

where $\Delta t \ll 1/f$ and $q(0, x) = -q_0 \,\mathrm{sign}(x)$.

This circulation can be viewed as a pair of gravity waves emanating from the origin and propagating respectively into the dry and moist regions. As the gravity waves propagate away from the origin at most at speed c_d, the temperature jump from Eq. (10) is spread over a region of length $\Delta x = c_d \Delta t$. This implies that the wind speed at the origin can be approximated by

$$u(0, \Delta t) \approx -\frac{q_0 \Delta t}{c_d \tau_c}. \tag{12}$$

The circulation is also associated with a net transport of water vapor across the origin given by

$$\begin{aligned} \int_0^\pi uq\,dz &= -\int_0^\pi u(x,t)\cos(z)[q(x,t) + \overline{Q}(z)]\,dz \\ &= u(x=0,t)\int_0^\pi [-\partial_z \overline{Q}(z)\sin(z)]\,dz = \tilde{Q}u. \end{aligned} \tag{13}$$

Here, we use the Galerkin approximation, in which $\overline{Q}(z)$ is the background moisture profile, $\cos(z)$ is the structure function for the horizontal velocity u, and the gross moisture stratification $\tilde{Q}$ is defined as the integral term in the second line. The atmospheric transport of water vapor is in the same direction as the low-level flow and is given by the term $\tilde{Q}u$. This accounts for the fact that the low-level flow from the dry region to the moist regions contains more water vapor than the return flow in the upper troposphere. That is, the initial precipitation sets up a direct circulation in which the low-level air flows from the dry region into the moist region ($u < 0$), which is associated with transport of water vapor from the dry region to the moist regions.

This water vapor transport further dries out the nonprecipitation region. Integrating the water vapor, Eq. (2) yields

$$\begin{aligned} \int_{0^+}^{c_d \Delta t} \partial_t q\,dx &= \tilde{Q}u(\Delta t, 0) \\ &\approx -\tilde{Q}\frac{q_0 \Delta t}{c_d \tau_c}, \end{aligned} \tag{14}$$

where the plus sign as a superscript indicates the region to the right of the origin. Similarly, the circulation transports water vapor into the moist region ($-c_d \Delta t$, 0):

$$\int_{-c_d \Delta t}^{0} (\partial_t q + P)\,dx \approx \tilde{Q}\frac{q_0 \Delta t}{c_d \tau_c}. \tag{15}$$

In the early stage of the adjustment (i.e., for $\Delta t < \tau_c$), this inflow of water vapor increases the water content in the moist regions. However, over longer time scales, precipitation has to prevail: the water vapor that was transported into the moist regions will be precipitated out. Equations (14) and (15) further indicate that the adjustment process brings moisture into the warm region ($x < 0$), which leads to enhanced precipitation. This initial circulation can be better understood with the schematic picture shown in Fig. 5. The arrows indicate the convective cell where the fluid flows toward the

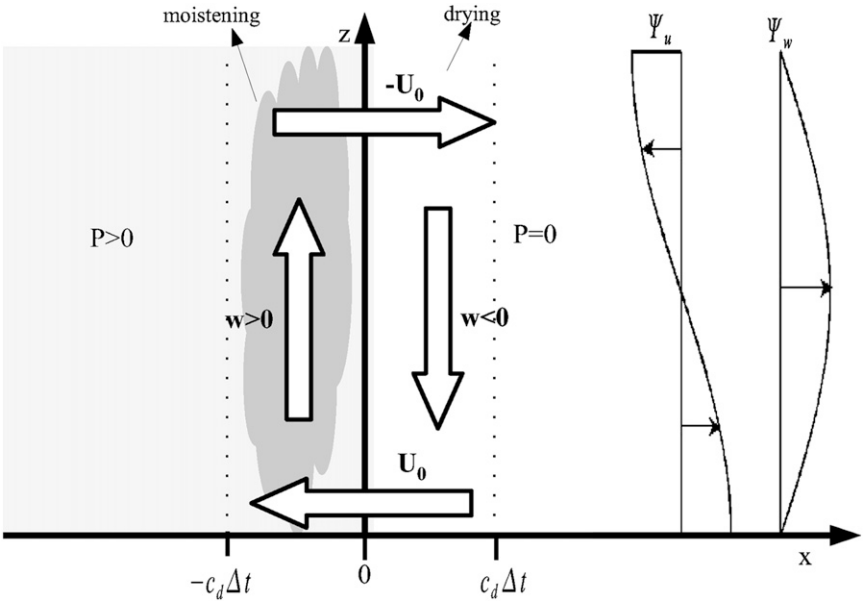

FIG. 5. Schematic representation of the initial adjustment process. The light gray region represents the initially supersaturated region and the dark gray area represents the precipitating region due to the initial inflow toward the moist region. The arrows represent the convective cell generated by the initial unbalanced moisture distribution. On the far right side the vertical structure function for u and w are displayed.

initially precipitating region at the surface, leading to more precipitation. The flow ascends to the left of the origin ($w = -\partial_x u$), turning back to the initially dry region. It then subsides, drying out the initially dry region.

Another interesting feature of the moist adjustment is that in the region where $q(x, 0) < 0$ the amplitude of oscillation of all variables are bounded throughout the integration time. As a result, when moisture starts sufficiently below saturation, it never reaches saturation (as shown in Fig. 1). Therefore, the final balanced solution in the dry region corresponds to the dry analytical solution, except that the temperature at the interface ($x = 0$) depends on the moist convective adjustment in the precipitating region.

Although these estimates hold for any τ_c, the results from the previous section and the dependence on τ_c in Eq. (15) suggest that the initially unbalanced flow evolves toward distinct final states in the slow or fast convective limits. This distinct behavior is discussed in sections 4b and 4c.

b. The slow convective limit

Because the precipitation dissipation rate is related to τ_c, precipitation is active for a long period of time when the convective adjustment time is long. In this section, we show that, as a result, in the slow convective limit, the distribution of the total amount of precipitating water $\langle P \rangle$ in the system can be estimated, as well as the final balanced flow. The argument is built on the fact that in this case the coupling between temperature and moisture is weak and after $t \gg 1/f$ time, most gravity wave activity must have propagated away from the region of interest, which implies that the convergence term $\partial_x u$ is small. Consequently, once all the water in the system has precipitated, variations in moisture are also small ($\partial_t q \approx \tilde{Q}\partial_x u$) and the final equilibrated moisture distribution has to be close to saturation. That is, $q_F \to 0$ when $\tau_c f \to \infty$.

More precisely, in section 2 we showed that in a region where precipitation is never active the dry PV is conserved and the balanced flow can be computed for any given initial state. Moreover, when the final moisture distribution is known, the final temperature can be determined because the moist PV is conserved. Hence, assuming $q_F = 0$, we can compute a solution in which the moist PV is conserved to the left of the origin and the dry PV is conserved to the right of it:

$$T_F(x) = \alpha e^{x/L_m} + T_I + q_I \quad \text{if} \quad x < 0, \tag{16}$$

$$T_F(x) = \beta e^{-x/L_d} - T_I \quad \text{if} \quad x \geq 0, \tag{17}$$

where $L_d = c_d/f$ is the dry Rossby radius, $L_m = c_m/f$ is the moist Rossby radius, and α and β are determined by matching the two solutions at the interface. For illustration, when $T_I + q_I = q_0$ if $x < 0$ and $T_I = 0$ if $x \geq 0$, we

have $\alpha = -[c_m/(1+c_m)]q_0$ and $\beta = [1/(1+c_m)]q_0$. This analytical solution will be referred as the moist-dry analytical solution. In particular, the moist-dry analytical solution shows that the temperature at the center of the channel is higher than it would be in the absence of precipitation,

$$T_F(0) = \frac{1}{1+c_m} q_0 > \frac{q_0}{2}, \tag{18}$$

and, using Eq. (9), the total precipitation is given by

$$\langle P \rangle(x) = \frac{1-c_m}{c_m} q_0 e^{x/L_m} \quad \text{if} \quad x < 0. \tag{19}$$

Figure 6 illustrates the close agreement between the moist-dry analytical and the numerical solution for large τ_c.

c. The fast convective limit

Here we show that the final state can also be estimated from the initial flow in the fast convective limit. Unlike the slow convective adjustment process where the precipitating region is stationary, the precipitating front moves westward in the fast limit. This process increases the amount of precipitation in the early stages of the adjustment, impacting the balanced flow. To obtain this estimate we first review some of the properties of the model in limit of small τ_c. The fast convective adjustment time in the absence of rotation has been discussed by FMP and Pauluis et al. (2008) and corresponds to the strict quasi-equilibrium (SQE) theory presented there. In SQE, moisture is instantaneously relaxed toward the saturation profile (in this case, to zero). That is, whenever moisture is above saturation,

$$q = \hat{q} = 0 \Rightarrow \partial_t q = 0 \Rightarrow P = -\tilde{Q}\nabla \cdot \mathbf{u} = -\tilde{Q}\partial_x u, \tag{20}$$

which implies that $\partial_t T = (1-\tilde{Q})\partial_x u$ when $P > 0$, and $\partial_t T = \partial_x u$ otherwise. The coupling between temperature and moisture tendencies is stronger and more likely to affect the geostrophic balanced solution since a precipitating region influences the dynamics of gravity waves. In particular, Pauluis et al. (2008) shows that gravity waves moving across precipitating and nonprecipitating regions can be treated as moving between regions of different refractive indices; therefore, waves are partially reflected and partially transmitted when they encounter the boundary between a moist and dry region. As previously mentioned, there is a clear distinction between the final states in the two limits; namely, in Fig. 3 a bump in temperature can be seen to the left of the initial discontinuity, which appears to be a result of the initial burst of precipitation in that region.

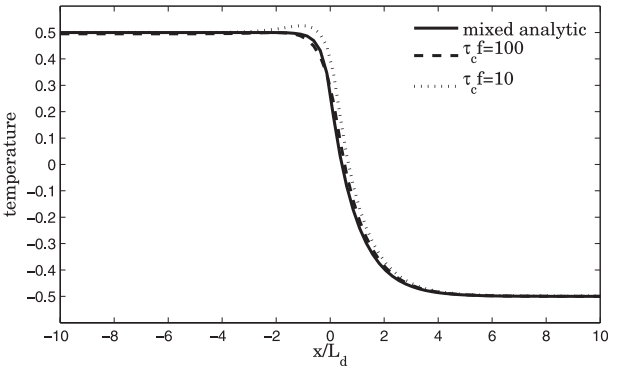

FIG. 6. Comparison between mixed analytical solution (solid line) and numerical solution for large τ_c (dashed and dotted lines).

To estimate the balanced flow, analogously to the slow adjustment process, we assume that precipitation exponentially decays with the moist Rossby radius,

$$\langle P \rangle(x) = \frac{P_0}{L_m} e^{x/L_m} \quad \text{if} \quad x < 0, \tag{21}$$

and this assumption is justified in the appendix. Inverting the dry PV Eq. (8a) we obtain a final temperature distribution that depends only on P_0. Note that to satisfy the moist PV equation in the initially moist portion of the channel, the final temperature has to depend on both dry and moist Rossby radius, whereas in the dry area it depends only on the dry Rossby radius. That is,

$$T_F(x) = \lambda e^{x/L_d} + \alpha e^{x/L_m} + q_0 \quad \text{if} \quad x < 0, \tag{22}$$

$$T_F(x) = \beta e^{-x/L_d} \quad \text{if} \quad x \geq 0. \tag{23}$$

To satisfy Eq. (8a) we obtain $\alpha = -[L_m L_d^2/(L_d^2 - L_m^2)]P_0$. The parameters λ and β are obtained assuming that the balanced temperature is continuous and differentiable at $x = 0$ and are functions of P_0. Note that the temperature at the interface must be warmer than in the dry adjustment:

$$T_F(0) = \frac{q_0}{2} + \frac{1}{1+c_m}\frac{P_0}{2}. \tag{24}$$

In addition, substituting the value for P_0 obtained in the previous section (when $\tau_c \to \infty$) results in $\lambda = 0$. Therefore, this formulation is consistent with the final temperature obtained for large τ_c. Interestingly, if P_0 is large enough, the matching temperature at the interface will be above the temperature away from the origin (in this case, q_0) and the final temperature will exhibit the bump observed in the numerical experiment.

In the appendix we derive in detail an estimate for P_0 that yields

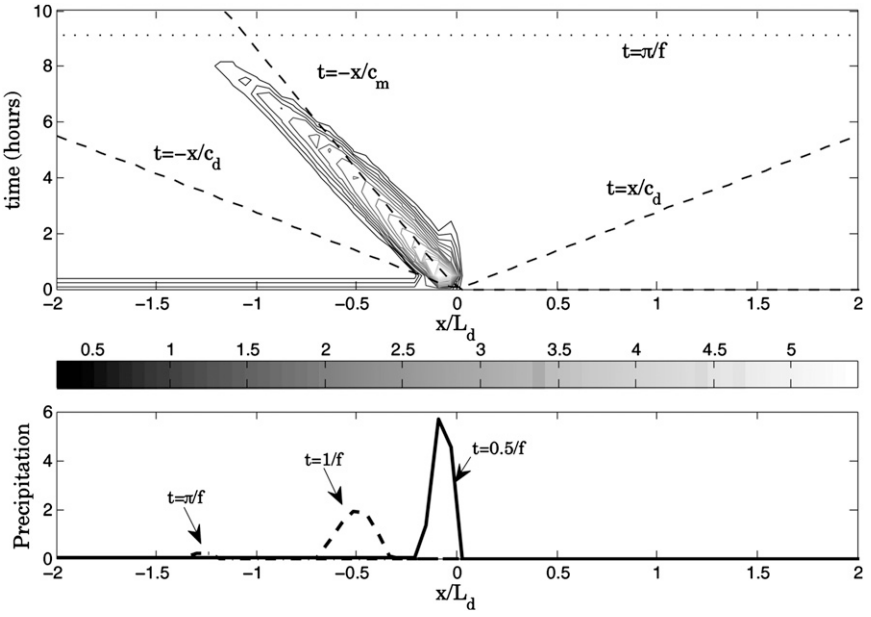

FIG. 7. (top) Time evolution of precipitation for short τ_c. The dashed lines correspond to the dry ($x = c_d t$) and moist ($x = c_m t$) characteristics, and the horizontal line corresponds to $t = \pi/f$. (bottom) Three snapshots (at $t = 0.5/f$, $1/f$, and π/f) of the precipitation amplitude.

$$P_0 \sim \frac{\tilde{Q} q_0}{(c_d + c_m)^2} \pi. \tag{25}$$

The argument presented there is built on the fact that in the limit of short τ_c, the precipitating region moves at speed c_m, as shown in Fig. 7 and illustrated in Fig. 8. Using the estimated value of P_0, we compute the final temperature distribution and total amount of precipitation, shown in Fig. 9. Notice the local maximum in temperature to the left of the origin. In the appendix it is shown that the extra amount of precipitation (in comparison to the slow convective adjustment) comes from the fact that since the precipitation region propagates westward, precipitation is not only generated by drying out the initially dry region, but also results from the contribution from the region between the moving precipitating front and the origin.

Notice that this analytical estimate does not account for the precipitation generated by gravity waves and thus it cannot explain the complete behavior of the balanced flow. For instance, the analytical solution exhibits a bump in temperature to the left of the origin; however, its amplitude is smaller and slightly shifted to the right in comparison to the numerical solution. Moreover, the total analytical precipitation underestimates the total numerical precipitation to the left of the origin and overestimates at the origin. Nevertheless, we showed that the basic features of the balanced flow are well represented, depending primarily on the initial adjustment process.

5. Conclusions

We presented a theoretical study of a geostrophic adjustment process in an idealized moist atmosphere where convection is represented by a Betts and Miller (1986) type of relaxation scheme. In particular, the case of a motionless flow evolving toward a balanced state was analyzed when only half of the domain is precipitating. A difference between the geostrophic adjustment in the dry and moist cases lies in that the moist adjustment process is associated with a water vapor transport from the dry regions to the moist regions that enhances the precipitation, sharpens the temperature gradient, and intensifies the jet. In this formulation, the gross moist stratification $\tilde{Q}$ determines the moist phase speed of the waves and, therefore, the length scale of the adjustment $L_m = \sqrt{1 - \tilde{Q}}/f$. Thus, the temperature front sharpens and the jet intensifies with decreasing values of $\tilde{Q}$.

A more fundamental difference rises from how gravity waves and the rotational flow interact in the two adjustment processes. On the one hand, in the dry case gravity waves do not affect the potential vorticity. This makes it possible to compute the final balanced state based solely on the initial potential vorticity distribution. On the other hand, in the moist case gravity waves

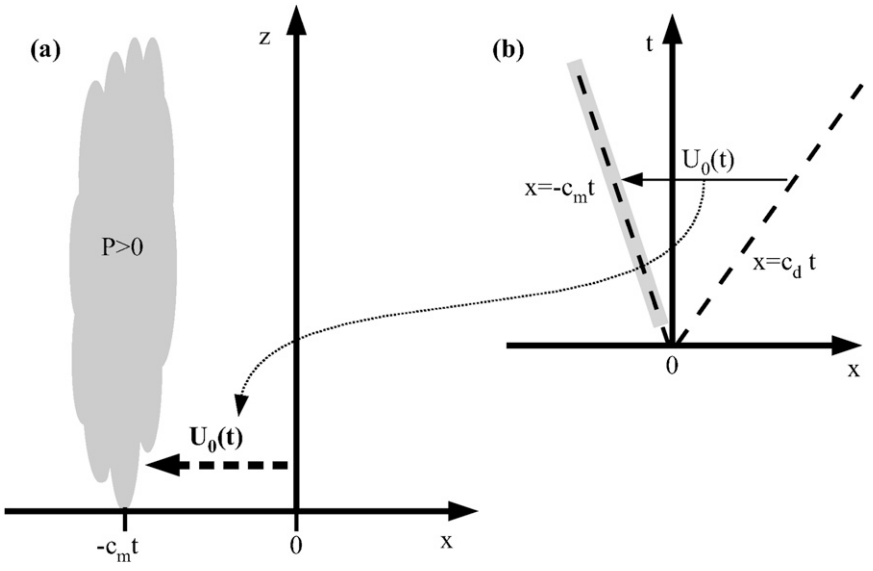

FIG. 8. Schematic representation of the precipitating region when $\tau_c \sim 0$, where $U_0(t)$ is the zonal flow at its edge at time t. (a) Precipitating region at time t in the (x, z) plane. (b) Precipitating region localized at $x = -c_m t$ in the x–t plane (schematic description of top panel in Fig. 7).

can generate precipitation, which in turn affects the potential vorticity distribution. This means that in the moist case the fast dynamics associated with the propagation of gravity waves can impact the slow dynamics tied to evolution of potential vorticity. As this coupling occurs through precipitation, one expects that details of the representation of convective processes should affect geostrophic adjustment in a moist atmosphere. This is evident in our numerical simulations from section 3, which show that adjusted flow strongly depends on the convective relaxation time.

To further understand the final flow dependence on the convective adjustment time, in section 4 analytical approximations are derived in two limits: the slow convective limit with $\tau_c f \gg 1$ and the fast convective limit with $\tau_c f \ll 1$. In the slow convective limit, the coupling through precipitation is weak, gravity waves propagate away from the origin, and the final solution converges to a solution similar to the analytical dry solution, but with a reduced length scale L_m in the initially supersaturated portion of the domain. In both cases precipitation is enhanced by the initial westward inflow, which dries out the initially dry region and moistens the initially moist region. In the slow convective limit, the right edge of the precipitating region is stationary and it is dissipated as gravity waves propagate away from the origin. In the fast case, the precipitating region propagates westward and more moisture is transported toward the precipitating region when compared to the slow case. The warming effect of this extra amount of precipitation produces a local maximum to the left of the origin in the final temperature distribution.

Our study emphasizes the fact that precipitation acts as a coupling mechanism between gravity waves and potential vorticity. In particular, the long-term evolution of the flow was shown to depend critically on the behavior of convection, which in our study could be characterized by a single nondimensional parameter $\tau_c f$. While our analysis is focused on a highly idealized problem and

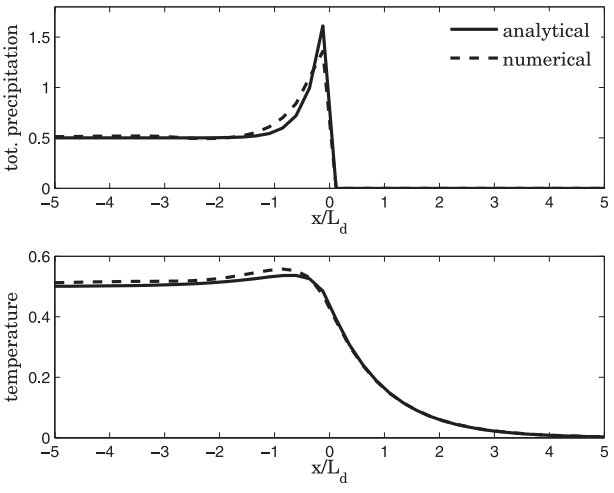

FIG. 9. (top) Comparison between the numerical (solid line) and the estimated (dashed line) total precipitation for small τ_c final temperature. (bottom) As in (top), but for the final temperature.

omits several other processes, such as radiation, evaporation, and vertical wind shear, our theoretical analysis provides a relatively simple framework to study the physical mechanisms by which precipitation affects geostrophic flows.

Acknowledgments. The comments of two reviewers are gratefully acknowledged, as they have considerably improved the clarity of this paper. Juliana Dias and Olivier Pauluis are supported by the NSF under Grant AGS-0545047.

APPENDIX

The Total Amount of Precipitation in the Fast Convective Limit

Here we present an estimate for the total amount of precipitation in the limit where $\tau_c \to 0$. The first assumption we make stands on the empirical evidence that the total amount of precipitation $\langle P\rangle(x)$ decays similarly in the fast and slow convective adjustment process (see Fig. 1a). Since in the case of the slow convective adjustment it was shown that $\langle P\rangle(x) \propto e^{-|x|/L_m}$, we assume that in the fast case $\langle P\rangle(x) = (P_0/L_m)e^{x/L_m}$ if $x < 0$, when τ_c is small, and we define the total amount of precipitation generated during the geostrophic adjustment process by

$$P_0 = \int_{-\infty}^{\infty}\int_0^{\infty} P(x,t)\,dt\,dx = \int_{-\infty}^{\infty}\langle P\rangle(x)\,dx. \quad \text{(A1)}$$

In the limit of τ_c infinitely small, moisture is relaxed toward saturation instantaneously; therefore, precipitation is generated and dissipated very rapidly. Since the initial zonal flow moves toward the moist portion of the domain, it must propagate at the moist gravity wave speed c_m, converging at $x = -c_m t$ where it generates a localized burst of precipitation. Thus, the precipitating region must be inside a region defined by $-c_m t \le x \le -c_m t + \delta$, where δ is a small positive distance (it corresponds to the gray area in Fig. 8b). Because precipitation is completely dissipated before the flow is balanced, it must satisfy

$$P_0 = \int_0^{t_0}\int_{-c_m t+\delta}^{-c_m t-\delta} P(x,\,t)\,dx\,dt, \quad \text{(A2)}$$

where t_0 will be determined later. Recall that in SQE, $P = -\tilde{Q}\partial_x u$; thus,

$$P_0 = -\tilde{Q}\int_0^{t_0} u(-c_m t - \delta,\,t)\,dt. \quad \text{(A3)}$$

We denote $U_0(t) = u(-c_m t - \delta, t)$, that is, the zonal flow at the right edge of the precipitating region (as the scheme in Fig. 8 indicates). Notice that to determine P_0, it is necessary to estimate both t_0 and U_0. To determine $U_0(t)$, we first derive the momentum budget equations

$$\partial_t \overline{U} = -\Delta T + f\overline{V}, \quad \text{(A4)}$$

$$\partial_t \overline{V} = f\overline{U}. \quad \text{(A5)}$$

Differentiation in time of Eq. (A4) and combining with Eq. (A5) yields

$$\partial_{tt}\overline{U} = -f^2\overline{U}, \quad \text{(A6)}$$

where $\overline{F} = \int_{-\infty}^{\infty} f\,dx$. Next, we make the following approximation:

$$u(x,t) = U_0(t) \quad \text{if} \quad -c_m t < x < c_d t,$$
$$0 \quad \text{otherwise;}$$

that is, the zonal wind is constant with respect to x between the characteristics $t = -x/c_m$ and $t = x/c_d$ (as illustrated in Fig. 8b). Computing the zonal average of $u(x, t)$, we obtain $\overline{U} = (c_d + c_m)tU_0(t)$ and substitution in Eq. (A6) yields

$$\partial_{tt}[(c_d + c_m)tU_0(t)] = -f^2(c_d + c_m)tU_0(t). \quad \text{(A7)}$$

The solution of the differential Eq. (A7) that satisfies $u(x, t) \to 0$ as $t \to 0$ is proportional to $\sin(ft)/(c_d + c_m)t$. To determine $U_0(0)$, we use Eq. (A4)

$$U_0'(t)t(c_m + c_d) + U_0(t)(c_m + c_d) = -\Delta T + fV_0(t)t(c_m + c_d)$$

and take the limit of $t \to 0$, which gives $U_0(0) = -\Delta T/(c_m + c_d)$. As a result

$$U_0(t) = -\frac{\Delta T}{(c_m + c_d)}\frac{\sin(ft)}{(c_d + c_m)t}.$$

Notice that $U_0(t)$ switches sign at $t_P = \pi/f$; since $P > 0$, we obtain

$$P_0 = \tilde{Q}\frac{q_0}{(c_m + c_d)^2}\int_0^{\pi/f}\frac{\sin(ft)}{t}dt \sim \frac{\tilde{Q}q_0}{(c_d + c_m)^2}\pi, \quad \text{(A8)}$$

where $\Delta T = q_0$. That is, using the estimate in (10) when $\Delta t = \tau_c$ implies that the initial discontinuity in temperature with moisture initially at saturation and the initial discontinuity in moisture with initially uniform temperature are equivalent in SQE.

REFERENCES

Arakawa, A., and W. H. Schubert, 1974: Interaction of a cumulus cloud ensemble with the large-scale environment, Part I. *J. Atmos. Sci.,* **31,** 674–701.

Betts, A. K., 1986: A new convective adjustment scheme. Part I: Observational and theoretical basis. *Quart. J. Roy. Meteor. Soc.,* **112,** 677–691.

——, and M. J. Miller, 1986: A new convective adjustment scheme. Part II: Single column tests using GATE wave, BOMEX, ATEX and arctic air-mass data sets. *Quart. J. Roy. Meteor. Soc.,* **112,** 693–709.

Blumen, W., 1972: Geostrophic adjustment. *Rev. Geophys. Space Phys.,* **10,** 485–528.

Dias, J., and O. Pauluis, 2009: Convectively coupled waves propagating along an equatorial ITCZ. *J. Atmos. Sci.,* **66,** 2237–2255.

Emanuel, K. A., J. D. Neelin, and C. S. Bretherton, 1994: On large-scale circulations in convecting atmospheres. *Quart. J. Roy. Meteor. Soc.,* **120,** 1111–1143.

Frierson, D. M. W., A. Majda, and O. Pauluis, 2004: Large scale dynamics of precipitation fronts in the tropical atmosphere: A novel relaxation limit. *Commun. Math. Sci.,* **2,** 591–626.

Gill, A. E., 1980: Some simple solutions for heat-induced tropical circulation. *Quart. J. Roy. Meteor. Soc.,* **106,** 447–462.

——, 1982: *Atmosphere–Ocean Dynamics*. Academic Press, 662 pp.

Khouider, B., and A. Majda, 2005a: A non-oscillatory balanced scheme for an idealized tropical climate model. Part I: Algorithm and validation. *Theor. Comput. Fluid Dyn.,* **19,** 331–354.

——, and ——, 2005b: A non-oscillatory balanced scheme for an idealized tropical climate model. Part II: Nonlinear coupling and moisture effects. *Theor. Comput. Fluid Dyn.,* **19,** 355–375.

Neelin, J. D., and N. Zeng, 2000: A quasi-equilibrium tropical circulation model—Formulation. *J. Atmos. Sci.,* **57,** 1741–1766.

Pauluis, O., A. Majda, and D. M. Frierson, 2008: Propagation, reflection and transmission of precipitation fronts in the tropical atmosphere. *Quart. J. Roy. Meteor. Soc.,* **124,** 913–930.

Rossby, C.-G., 1938: On the mutual adjustment of pressure and velocity distributions in certain simple current systems. *J. Mar. Res.,* **1,** 239–263.

Silva Dias, P. L., W. H. Schubert, and M. DeMaria, 1983: Large-scale response of the tropical atmosphere to transient convection. *J. Atmos. Sci.,* **40,** 2689–2707.

Stechmann, S., and A. Majda, 2006: The structure of precipitation fronts for finite relaxation time. *Theor. Comput. Fluid Dyn.,* **20,** 377–404.